# Model framework for emergence of synchronized oscillations

Kei-Ichi Ueda ⬡

*Graduate School of Science and Engineering, University of Toyama, Toyama 930-8555, Japan*

Autonomy is an important concept when investigating the mechanism whereby biological systems exhibit flexibility against unpredictable environmental changes. Herein we propose a parameter-tuning algorithm, based on a selection principle, that allows the emergence of synchronization between populations of oscillators through autonomous changes of the intrinsic parameters. With the algorithm, the populations exhibit self-recovery of the synchronized state after the existing synchronized state is broken suddenly; that is, the system chooses appropriate values of the intrinsic parameters to recover the synchronized state. We also propose a continuous model in which the selection is described by the replicator model and the parameter values are determined by the density profile of the oscillators in parameter space.

## I. INTRODUCTION

Elucidating the mechanism for adaptability in biological systems is an important problem in biological sciences. Although biological systems comprise many elements (e.g., cells and organs), the behaviors of the elements are well organized beyond the hierarchy of scale to adapt to environmental changes.

Modeling studies have been conducted to clarify the mechanism for adaptability. When constructing models based on differential equations, one approach is to assume that the system has multiple attractors and that adaptive behavior arises from switching among those attractors; a typical example of this approach is the Hopfield model [1]. Another approach is to assume that the system changes the values of its intrinsic parameters appropriately according to environmental changes. In that approach, the system has a parameter-tuning system that receives information from the environment and outputs appropriate parameter values to recover the system's performance. In the present study, we propose a model framework for a parameter-tuning system based on the latter modeling approach, in which the following difficulty arises frequently. If the external parameter-tuning system depends on variables derived from the environment, then the system cannot give appropriate outputs when it encounters an unknown environment. Consequently, so that the system can adapt to an unknown environment, the parameter-tuning algorithm should be independent of any and all environmental variables. Herein we consider the simple question of whether it is possible to construct a parameter-tuning algorithm that is independent of external systems. Theoretical study of this simple question should motivate new experimental studies involving biological evolution and contribute to elucidating the mathematical mechanism for how biological systems change their intrinsic dynamics through the evolution process to adapt to environmental changes.

In this paper, we investigate an autonomous parameter-tuning system that stabilizes synchronized oscillations. To describe our motivation, we introduce the coupled oscillator system

$$
\begin{aligned}
\dot{u}_1 &= \mu u_1 - \omega v_1 - (u_1^2 + v_1^2)u_1 + \eta_1 u_2, \\
\dot{v}_1 &= \omega u_1 + \mu v_1 - (u_1^2 + v_1^2)v_1 + \eta_1 v_2, \\
\dot{u}_2 &= \mu u_2 - \omega v_2 - (u_2^2 + v_2^2)u_2 + \eta_2 u_1, \\
\dot{v}_2 &= \omega u_2 + \mu v_2 - (u_2^2 + v_2^2)v_2 + \eta_2 v_1,
\end{aligned}
\tag{1}
$$

where $\mu, \omega \in \mathbb{R}$ and the overdot denotes the derivative with respect to time $t$. We refer to the $(u_1, v_1)$ equations and the $(u_2, v_2)$ equations as systems 1 and 2, respectively. By means of the coordinate changes $u_k = r_k \cos \theta_k$ and $v_k = r_k \sin \theta_k$, Eq. (1) becomes

$$
\begin{aligned}
\dot{r}_1 &= \mu r_1 - r_1^3 + \eta_1 r_2 \cos(\theta_2 - \theta_1), \\
\dot{\theta}_1 &= \omega + \eta_1 \frac{r_2}{r_1} \sin(\theta_2 - \theta_1), \\
\dot{r}_2 &= \mu r_2 - r_2^3 + \eta_2 r_1 \cos(\theta_1 - \theta_2), \\
\dot{\theta}_2 &= \omega + \eta_2 \frac{r_1}{r_2} \sin(\theta_1 - \theta_2).
\end{aligned}
\tag{2}
$$

Thus, by taking $\phi := \theta_1 - \theta_2$ we have

$$
\dot{\phi} = -\left( \frac{r_2}{r_1} \eta_1 + \frac{r_1}{r_2} \eta_2 \right) \sin \phi.
$$

We find that $\lim_{t \to \infty} \phi \to 0$ when $\eta_1 > 0$ and $\eta_2 > 0$ and that $\lim_{t \to \infty} \phi \to \pm \pi$ when $\eta_1 < 0$ and $\eta_2 < 0$. In addition, $\lim_{t \to \infty} r_k = \sqrt{\eta_k + \mu}$ if $\eta_k + \mu > 0$ ($k = 1, 2$). These calculations indicate that phase-synchronized oscillation between systems 1 and 2 occurs when the signs of $\eta_1$ and $\eta_2$ are the same; we have in-phase (antiphase) oscillation for $\eta_k > 0$ ($\eta_k < 0$) when $\eta_k + \mu > 0$ ($k = 1, 2$). When $\eta_2$ is fixed, we consider the following two questions: (i) What should the dynamics of $\eta_1$ be such that systems 1 and 2 exhibit synchronized oscillations and (ii) when the sign of $\eta_2$ is changed abruptly, how does system 1 sense that change and change the sign of $\eta_1$ to generate synchronized oscillations? These questions are easy to answer if system 1 can observe system 2 and knows the value of $\eta_2$. For example, a possible

answer is

$$\dot{\eta}_1 = \eta_2 - \eta_1.$$

In addition, if system 1 can observe the phase of system 2 or $(u_2, v_2)$ online, then questions (i) and (ii) are answered. In fact, model equations involving the time evolution of the connectivity between the oscillators have been proposed previously [2–7]; in those studies, the time evolution was described as a function of the phase difference between the oscillators. Furthermore, the self-organization of characteristic network structures (including scale-free networks) through coevolution of the network structure and dynamical features has been investigated [8,9]. Most of the models in such studies assume that the connection (edge) weight dynamics are determined by two oscillators connected to the edge. Algorithms for controlling the synchronization of chaotic oscillators [10–12] and control methods for synchronized oscillatory patterns [13,14] have been investigated. However, because the purpose of this study is to derive a parameter-tuning system that can be described without using variables of the external systems, such previous model frameworks are not applicable here.

Improving system adaptability is an important issue in not only biological systems but also engineering. For instance, when a robot encounters an unpredicted environmental change, the system must find appropriate parameter values to achieve systemwide functionality. Automatic parameter control inspired by self-organized dynamics has been applied to robotics. The advantage of using a dynamical system is that the system can change an attractor flexibly according to the external perturbation or environmental change. Examples of this include bipedal locomotion in an unpredictable environment [15] and frequency control using resonance [16,17]. In the present study, we show that (i) synchronized oscillations appear spontaneously as a result of self-organized dynamics and (ii) our proposed model concept can also be applied to an automatic parameter-tuning algorithm for a locomotion system.

## II. SIMPLE MODEL

Herein we consider hierarchical coupled oscillator systems, the framework of which has been investigated for several decades in biological sciences, including neural networks and cell-cell interactions [18,19]. In particular, we investigate interactions between populations of oscillators (Fig. 1). We refer to the $k$th population as $P_k$. The model has the following properties: (i) The populations are coupled by a mean-field interaction; (ii) each oscillator in the population possesses parameters whose values are updated by a parameter-tuning algorithm; (iii) the algorithm used in (ii) for $P_k$ involves only variables of the oscillators belonging to $P_k$.

Note that the algorithm to control the parameter values of the oscillators in $P_k$ is formulated using only the variables of those oscillators and none corresponding to the other populations; that is, the algorithm uses only local variables.

We begin by proposing a simple model for the parameter-tuning algorithm; then we propose a continuous version of the simple model. For both models, we use an algorithm based on a selection principle. For this we define an order parameter and propose a selection algorithm.
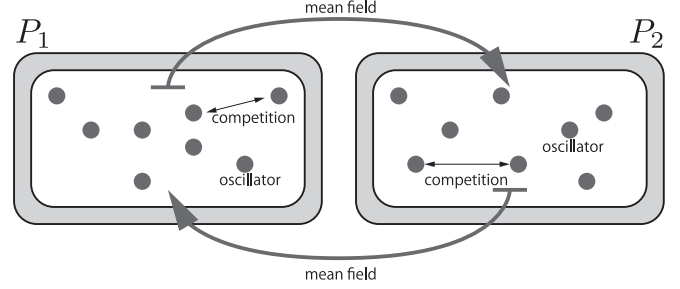


FIG. 1. Framework of the two-population model. Each population contains oscillator elements. Selection occurs through the competition between elements. Populations $P_1$ and $P_2$ interact through a mean field.

### A. Simple model: Single parameter

#### 1. Population dynamics

The dynamics of oscillator $j$ in population $k$ ($P_k$) are described by

$$\dot{\boldsymbol{u}}_k^{(j)} = \boldsymbol{F}(\boldsymbol{u}_k^{(j)}; \omega) + C \sum_{l=1, l \neq k}^{K} \eta_{lk}^{(j)} \boldsymbol{U}_l + \boldsymbol{U}_k^{\mathrm{ptb}} + A\boldsymbol{W}_k(t),$$

$$\boldsymbol{U}_k = {}^t(\bar{u}_k, \bar{v}_k), \tag{3}$$

$$\bar{u}_k = \frac{1}{J} \sum_{j=1}^{J} u_k^{(j)}, \quad \bar{v}_k = \frac{1}{J} \sum_{j=1}^{J} v_k^{(j)},$$

where $t \in (0, T]$, $\boldsymbol{u}_k^{(j)} = {}^t(u_k^{(j)}, v_k^{(j)})$, $k = 1, 2, \dots, K$, and $j = 1, 2, \dots, J$. Here $J$ is the number of oscillators in $P_k$, $C$ and $A$ are positive constants, $\omega$ is the angular frequency, and $\boldsymbol{U}_k^{\mathrm{ptb}}$ represents external perturbations. We add a noise $\boldsymbol{W}_k = {}^t(W_k^u, W_k^v)$, where $W_k^*$ ($* = u, v$) is Gaussian noise with zero mean and unit variance. We use a typical oscillator model, namely, $\boldsymbol{F}(\boldsymbol{u}_k^{(j)}; \omega) := {}^t(f(u_k^{(j)}, v_k^{(j)}; \omega), g(u_k^{(j)}, v_k^{(j)}; \omega))$, where $f(u, v; \omega) := \mu u - \omega v - (u^2 + v^2)u$ and $g(u, v; \omega) := \omega u + \mu v - (u^2 + v^2)v$. The parameter $\eta_{lk}^{(j)}$ determines the sign and strength of the signal from $P_l$ to $P_k$, which are taken as time-dependent variables unless stated otherwise.

#### 2. Order parameter

Because our algorithm is based on selection of elements, we define an order parameter to evaluate an element's state, and selection occurs according to the rank of the order parameter. We use a simple order parameter, namely, the time average of the amplitude of the oscillators, to evaluate the goodness of the parameter values. We suppose that the order parameter is updated every period $\tau$. That is, the order parameter of element $j$ in population $k$ for $t \in [(m-1)\tau, m\tau]$ ($m = 1, 2, \dots$) is defined by

$$S_k^{(j)}(m) = \frac{1}{\tau} \int_{(m-1)\tau}^{m\tau} \sqrt{\left(u_k^{(j)}\right)^2 + \left(v_k^{(j)}\right)^2} \, dt, \tag{4}$$

where $\tau$ is the updating period.
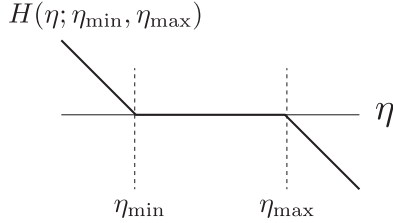
FIG. 2. Schematic of the function $H$.

### 3. Selection

The dynamics of the parameters are described by differential equations. We introduce our algorithm for $\eta_{lk}^{(j)}$ as an example, but it is the same for the other parameters. We assume that the parameter values vary (i) as a random walk and (ii) because of the selection algorithm. The random-walk process is described by

$$\dot{\eta}_{lk}^{(j)} = H\big(\eta_{lk}^{(j)}; \eta_{\min}, \eta_{\max}\big) + A_\eta W(t),$$

$$H(\eta; \eta_{\min}, \eta_{\max}) = (\eta_{\min} - \eta)_+ - (\eta - \eta_{\max})_+, \qquad (5)$$

$$(x)_+ = \begin{cases} x & \text{if } x > 0 \\ 0 & \text{otherwise,} \end{cases}$$

where $A_\eta$ is a positive constant and $W$ is Gaussian noise with zero mean and unit variance. We introduce the first term on the right-hand side to prevent the parameters from diverging in practice (Fig. 2). The parameters $\eta_{\min}$ and $\eta_{\max}$ determine the boundaries of $\eta_{lk}^{(j)}$.

For the selection process, we assume simply that the parameter values in the same population are replaced at $t = m\tau$ $(m = 1, 2, \dots)$ by those of the best element. That is,

$$\eta_{lk}^{(j)}(m\tau) = \eta_{lk}^{(j_k^*)}(m\tau), \qquad (6)$$

where $j = 1, 2, \dots, J$, $l \in \{1, 2, \dots, K\} \backslash \{k\}$, and $j_k^* = \arg\max_j S_k^{(j)}(m)$.

### 4. Loop network structure

In the present study, the selection algorithm is described by the variables belonging to the corresponding population and is independent of the variables of the other populations. This means that evaluating the goodness of the parameter values requires feedback from the other populations. Therefore, we suppose that the interaction network among populations has a loop structure.

### 5. Parameters

We take values of the parameters $\mu$, $\eta_{\min}$, and $\eta_{\max}$ such that each oscillator (i) exhibits large-amplitude oscillation when synchronization occurs between the populations and (ii) converges to a stationary state when synchronization does not occur: $\mu = -1.0 \times 10^{-4}$, $\eta_{\min} = -1$, and $\eta_{\max} = 1$. The parameter $\tau$ is set to 100. Because we take values of $\omega$ between 1.0 and 2.0, those of $\tau$ range from approximately 16 to 32 times the oscillator period. Once all the oscillators have approached the stationary state (or $U_l = 0$), no further oscillatory motion appears because $\mu < 0$. By taking $A > 0$, it is observed that the oscillatory motion recovers after all the

oscillators have approached the stationary state. Thus, we take $A = 0.004$.

### B. Results: Single parameter

We consider a two-population model ($K = 2$) and vary $\eta_{lk}^{(j)}$ in Eq. (3) according to the algorithm given by Eqs. (5) and (6). As a numerical scheme, the explicit Euler-Maruyama method is used. For notational convenience, we define $\eta_1^{(j)} := \eta_{21}^{(j)}$ and $\eta_2^{(j)} := \eta_{12}^{(j)}$ ($j = 1, \dots, J$). From analysis of Eq. (2), each oscillator exhibits large-amplitude in-phase and antiphase synchronization when $(\eta_1^{(j)}, \eta_2^{(j)}) = (+1, +1)$ $[=(\eta_{\max}, \eta_{\max})]$ and $(\eta_1^{(j)}, \eta_2^{(j)}) = (-1, -1)$ $[=(\eta_{\min}, \eta_{\min})]$, respectively, for all $j$. Because the phase differences among the oscillators in the same population tend to vanish, two types of synchronization occur simultaneously, namely, intrapopulation synchronization and interpopulation synchronization. Specifically, intragroup synchronization occurs if and only if intergroup synchronization occurs.

To examine the performance of the algorithm, we investigate the following two cases. In case 1, the dynamics of $\eta_1^{(j)}$ are described by Eqs. (5) and (6) whereas those of $\eta_2^{(j)}$ are fixed at $+1$ or $-1$. In case 2, the dynamics of $\eta_1^{(j)}$ and $\eta_2^{(j)}$ are described by Eqs. (5) and (6). In case 1, we also confirm that our algorithm exhibits self-recovery of synchronization when the sign of $\eta_2^{(j)}$ is changed suddenly. In case 2, we confirm that the parameters $\eta_k^{(j)}$ vary such that excitatory-excitatory (EE) or inhibitory-inhibitory (II) interaction occurs spontaneously. In addition, we confirm that transitions between EE and II interaction occur when external perturbations are applied. More precisely, we confirm that $\eta_k^{(j)}$ switches from $+1$ ($-1$) to $-1$ ($+1$) when $P_1$ and $P_2$ are forced to switch from in-phase (antiphase) to antiphase (in-phase) synchronization.

### 1. Case 1

We take $\eta_2^{(j)} \equiv +1$ for $t \leqslant T/2$ and $\eta_2^{(j)} \equiv -1$ for $t > T/2$ for all $j$. We expect $\eta_1^{(j)}$ (i) to approach $+1$ for $t \leqslant T/2$ and for there to be EE interactions between the populations and (ii) to approach $-1$ for $t > T/2$ and for there to be II interactions between the populations. Figure 3(a) shows the time sequences of $\bar{\eta}_1$ and $\bar{\eta}_2$, where $\bar{\eta}_k := \sum_j \eta_k^{(j)}/J$. The sign of $\bar{\eta}_1$ changed from positive to negative around $t = T/2$, thereby indicating that the algorithm chose the sign of $\eta_1^{(j)}$ successfully and that there were stable synchronized oscillations between $P_1$ and $P_2$.

### 2. Case 2

Next we consider the case in which the dynamics of $\eta_1^{(j)}$ and $\eta_2^{(j)}$ are governed by the algorithm [Eqs. (5) and (6)]. We consider the following questions.

(i) Does the system exhibit autonomous in-phase or antiphase synchronization through the mean-field interactions between $P_1$ and $P_2$?

(ii) Do the signs of $\eta_1^{(j)}$ and $\eta_2^{(j)}$ change autonomously from EE to II interaction or from II to EE interaction when the oscillator phase difference between $P_1$ and $P_2$ is forcibly changed?
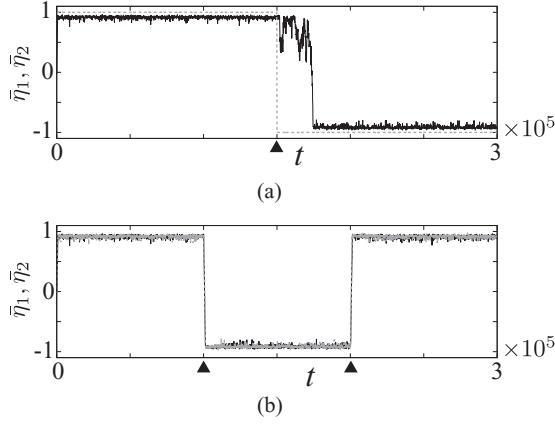
FIG. 3. Black and gray lines indicate time sequences of $\bar{\eta}_1$ and $\bar{\eta}_2$, respectively. Perturbations are applied at the times indicated by the closed black triangles: (a) $t = T/2$ and (b) $t = t_1, t_2$. We set $T = 3.0 \times 10^5$, $J = 20$, $\omega = 1.0$, $C = 0.05$, $A_\eta = 0.01$, and $\tau = 100$. (a) $\eta_2^{(j)}$ is changed from $+1$ to $-1$ at $t = T/2$. (b) External perturbation given by Eq. (7) is applied.

For question (ii), we expect the signs of $\eta_1^{(j)}$ and $\eta_2^{(j)}$ to become positive (negative) when in-phase (antiphase) synchronization occurs between $P_1$ and $P_2$. It is well known that the sign of $\eta_k^{(j)}$ determines the phase difference between $P_1$ and $P_2$. However, question (ii) asks whether the phase difference between $P_1$ and $P_2$ can change the sign of $\eta_k^{(j)}$.

To control the phase difference between in-phase and antiphase synchronizations, we add to the system the perturbations

$$U_k^{\mathrm{ptb}} = \begin{cases} {}^t(10 \ \sin(\omega' t - \theta_k), 0) & \text{if } t \in [t_1, t_1 + t_\delta] \\ {}^t(10 \ \sin(\omega' t - \theta_k'), 0) & \text{if } t \in [t_2, t_2 + t_\delta] \\ {}^t(0, 0) & \text{otherwise,} \end{cases} \quad (7)$$

where we set $t_1 = T/3$, $t_2 = 2T/3$, $t_\delta = 1.0 \times 10^4$, $\omega' = 2$, $(\theta_1, \theta_2) = (0, \pi)$, and $(\theta_1', \theta_2') = (0, 0)$. Because of Eq. (7), antiphase and in-phase synchronizations are induced for $t \in [t_1, t_1 + t_\delta]$ and $t \in [t_2, t_2 + t_\delta]$, respectively.

Figure 3(b) shows that the signs of $\eta_1^{(j)}$ and $\eta_2^{(j)}$ change from positive to negative around $t = t_1$ and from negative to positive around $t = t_2$. Consequently, the system exhibits stable antiphase and in-phase synchronizations for $t \in [t_1 + t_\delta, t_2]$ and $t \in [t_2 + t_\delta, T]$, respectively. This indicates that the algorithm changes the parameters flexibly according to the phase difference between $P_1$ and $P_2$.

### 3. Four populations: Application to a central pattern generator system

The algorithm can be applied to systems involving multiple populations, a typical example being a central pattern generator of animal gait patterns. The mathematical mechanism for the gait transition in response to perturbations has been investigated (e.g., [20]). Here we investigate case 2 as discussed in the two-population model. That is, we consider whether the algorithm can control the sign of $\eta_{lk}^{(j)}$ according to the phase difference between populations for a four-population system shown in Fig. 4(a); we set $\eta_{13}^{(j)} = \eta_{31}^{(j)} = \eta_{24}^{(j)} = \eta_{42}^{(j)} \equiv 0$ for all $j$.
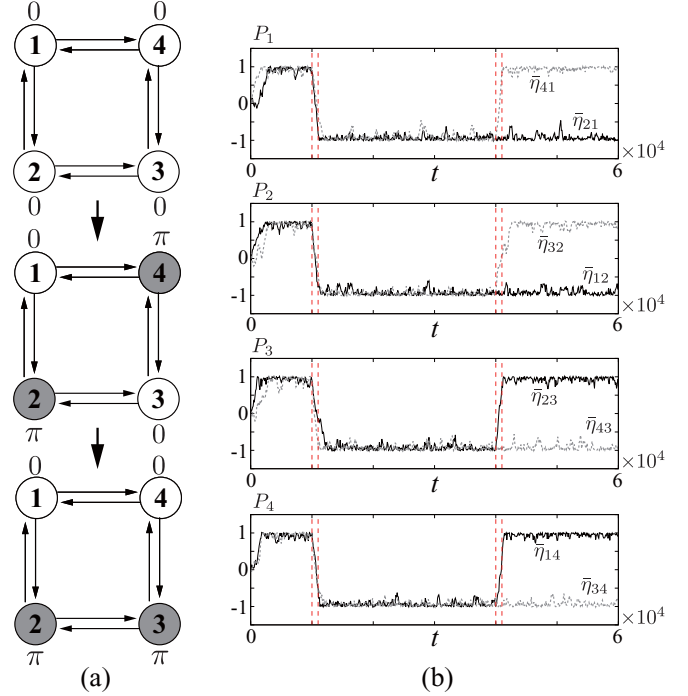


FIG. 4. (a) Phase differences of populations 1–4 for $t < t_1$ (top), $t \in (t_1 + t_\delta, t_2)$ (middle), and $t > t_2 + t_\delta$ (bottom). Arrows indicate interaction networks with $\eta_{lk} \not\equiv 0$. (b) Time sequences of $\bar{\eta}_{lk}$. The parameters are set to $T = 6.0 \times 10^4$, $J = 20$, $\omega = 1.0$, $C = 0.05$, $A_\eta = 0.01$, and $\tau = 100$.

We show that the population can undergo a transition by adding the external perturbation

$$U_k^{\mathrm{ptb}} = \begin{cases} {}^t(0.5 \ \sin(\omega' t - \theta_k), 0) & \text{if } t \in [t_1, t_1 + t_\delta] \\ {}^t(0.5 \ \sin(\omega' t - \theta_k'), 0) & \text{if } t \in [t_2, t_2 + t_\delta] \\ {}^t(0, 0) & \text{otherwise,} \end{cases}$$

where $t_1 = T/3$, $t_2 = 2T/3$, $t_\delta = 1000$, $\omega' = 2$, $(\theta_1, \theta_2, \theta_3, \theta_4) = (0, \pi, 0, \pi)$, and $(\theta_1', \theta_2', \theta_3', \theta_4') = (0, \pi, \pi, 0)$. We expect the signs of $(\eta_{12}, \eta_{23}, \eta_{34}, \eta_{41})$ $[(\eta_{21}, \eta_{32}, \eta_{43}, \eta_{14})]$ to switch to $(-, -, -, -)$ and $(-, +, -, +)$ around $t = t_1$ and $t_2$, respectively. Similar to the results in Fig. 3(b), the sign of $\bar{\eta}_{lk}$ changes according to the oscillator phase difference, where $\bar{\eta}_{lk} := \sum_j \eta_{lk}^{(j)}/J$. In fact, as shown in Fig. 4(b), $P_1$-$P_3$ and $P_2$-$P_4$ exhibit in-phase synchronization and $P_1$-$P_2$ and $P_3$-$P_4$ exhibit antiphase synchronization for $t \in [t_1 + t_\delta, t_2]$, and $P_1$-$P_4$ and $P_2$-$P_3$ exhibit in-phase synchronization and $P_1$-$P_2$ and $P_3$-$P_4$ exhibit anti-phase synchronization for $t \in [t_2 + t_\delta, T]$. This means that the parameter values are selected appropriately, as was observed in the two-population model.

### C. Simple model: Multiple parameters

The algorithm can be used to control multiple parameters. In addition to $\eta_{lk}^{(j)}$, we take $\omega$ in Eq. (3) as a control parameter. That is, we consider the following equation:

$$\dot{u}_k^{(j)} = F\left(u_k^{(j)}; \omega_k^{(j)}\right) + C \sum_{l=1, l \neq k}^{K} \eta_{lk}^{(j)} U_l + A W(t). \quad (8)$$

We consider a two-population model ($K = 2$) and we define $\eta_1^{(j)} := \eta_{21}^{(j)}$ and $\eta_2^{(j)} := \eta_{12}^{(j)}$ ($j = 1, \ldots, J$). Similar to Eq. (5), the time evolution of $\eta_k^{(j)}$ and that of $\omega_k^{(j)}$ are described by

$$\dot{\eta}_k^{(j)} = H\big(\eta_k^{(j)}; \eta_{\min}, \eta_{\max}\big) + A_\eta W(t),$$
$$\dot{\omega}_k^{(j)} = H\big(\omega_k^{(j)}; \omega_{\min}, \omega_{\max}\big) + A_\omega W(t), \qquad (9)$$

where we take $\eta_{\min} = -1.0$, $\eta_{\max} = 1.0$, $\omega_{\min} = 1.0$, and $\omega_{\max} = 2.0$. The algorithm for selecting $\eta_k^{(j)}$ and $\omega_k^{(j)}$ is given by

$$\eta_k^{(j)}(m\tau) = \eta_k^{(j_k^*)}(m\tau),$$
$$\omega_k^{(j)}(m\tau) = \omega_k^{(j_k^*)}(m\tau), \qquad (10)$$

where $j = 1, 2, \ldots, J$; $k = 1, 2$; $m = 1, 2, \ldots$; and $j_k^* = \arg\max_j S_k^{(j)}(m)$.

### D. Results: Multiple parameters

We investigate two cases. In case 1, the dynamics of $\eta_1^{(j)}$ and $\omega_1^{(j)}$ are described by Eqs. (9) and (10) while $\eta_2^{(j)}$ and $\omega_2^{(j)}$ are taken as the constants $\eta_2^*$ and $\omega_2^*$, respectively. As a perturbation, we change $\eta_2^*$ and $\omega_2^*$ from $+1$ to $-1$ and from 1.3 to 1.7, respectively, at $t = T/2$. In case 2, the dynamics of $\eta_1^{(j)}$, $\eta_2^{(j)}$, $\omega_1^{(j)}$, and $\omega_2^{(j)}$ are described by Eqs. (9) and (10). As a perturbation, we apply Eq. (7).

In case 1, we expect $\eta_1^{(j)}$ and $\omega_1^{(j)}$ to approach $\eta_2^*$ and $\omega_2^*$, respectively. Figure 5(a) shows that $\bar{\eta}_1$ and $\bar{\omega}_1$ successfully approach $\eta_2^* = 1.0$ and $\omega_2^* = 1.3$, respectively. In case 2, we observe that $\eta_1^{(j)}$ and $\omega_1^{(j)}$ have almost the same values as $\eta_2^*$ and $\omega_2^*$, respectively. Note that because the amplitude of the oscillation in Eq. (1) is independent of $\omega$ when $(\eta_1, \eta_2) = (+1, +1)$ or $(\eta_1, \eta_2) = (-1, -1)$, the order parameter $S_k^{(j)}$ is independent of $\omega_k^{(j)}(t)$ if all of $\omega_1^{(j)}(t)$ and $\omega_2^{(j)}(t)$ ($j = 1, 2, \ldots, J$) have the same values for all $t$. Because of this property of translation invariance, the time sequences of $\bar{\omega}_1$ and $\bar{\omega}_2$ fluctuate. However, their values remain approximately the same for the entire time, which implies that the system successfully chooses the optimal parameter values.

### E. Self-recovery mechanism and parameter dependence

The autonomous parameter tuning after the perturbations (sudden parameter changes and external forces) of the two-population system is completed through the following four steps: (i) From the perturbations, both $|\boldsymbol{U}_1|$ and $|\boldsymbol{U}_2|$ decrease because of the inharmonic oscillations; (ii) $S_k^{(j)}$ decreases for all $j$ and $k$; (iii) the distribution of parameters in each population becomes larger, thereby increasing the flexibility regarding the choice of parameter values; (iv) the optimal parameter is selected from the various options.

We use loop interaction networks because processes (i) and (ii) are driven by the mutual interaction between $P_1$ and $P_2$. Desynchronization of $P_1$ decreases the degree of synchronization of $P_2$ and vice versa. This indicates that the desynchronization of oscillators in each population is important for the self-recovery property. We therefore add noise to the oscillators such that intrapopulation desynchronization
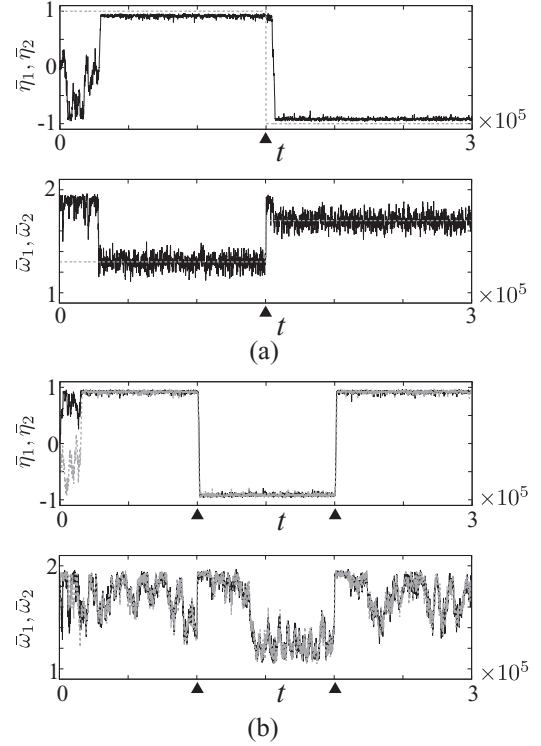


FIG. 5. Solid black lines indicate the time sequences of $\bar{\eta}_1$ and $\bar{\omega}_1$ and dashed gray lines indicate the time sequences of $\bar{\eta}_2$ and $\bar{\omega}_2$. Triangles indicate the beginning of the perturbations: (a) $t = T/2$ and (b) $t = t_1$ and $t_2$. The parameters are set to $T = 3.0 \times 10^5$, $J = 20$, $\omega = 1.0$, $C = 0.2$, $A_\eta = 0.01$, $A_\omega = 0.01$, and $\tau = 100$.

occurs when interpopulation desynchronization occurs. Qualitatively the same process takes place for the four-population model.

The amplitude of the noise ($A_\eta$ and $A_\omega$) crucially affects the self-recovery performance. So that the system robustly chooses appropriate parameter values after the perturbations, the distribution of the parameters in each population [process (iii)] should be large. That is, the noise amplitude should be large. In fact, the self-recovery fails for small noise amplitude [Fig. 6(a)]. By contrast, the fluctuation of the time series of $\eta_k^{(j)}$ tends to increase with the noise amplitude [Fig. 6(c)]. Therefore, the noise amplitude should be taken in an appropriate regime [Fig. 6(b)].

Numerically, we find qualitatively the same behavior for a large number of oscillators. Indeed, we observe self-recovery for $J = 100$ with the same parameter values [Figs. 6(d)–6(f)].

The parameter $\tau$ should be given in an appropriate regime. Figure 7(a) shows examples of time sequences of Eq. (3) with perturbation (7) when $\tau$ is changed. When $\tau$ is smaller than the period of $\boldsymbol{u}_k^{(j)}$ ($\tau = 4$), the degree of synchronization decreases [Fig. 7(a)]. When $\tau = 4000$, which is larger than 100 times the period of $\boldsymbol{u}_k^{(j)}$, the behavior of $\bar{\eta}_j$ fluctuates, while the synchronized state can be maintained.

In our algorithm, the parameter values in the same population are assumed to be replaced at $t = m\tau$ ($m = 1, 2, \ldots$) by those of the best element. We can find qualitatively the same behavior as that shown in Fig. 3(b) when algorithm (6)
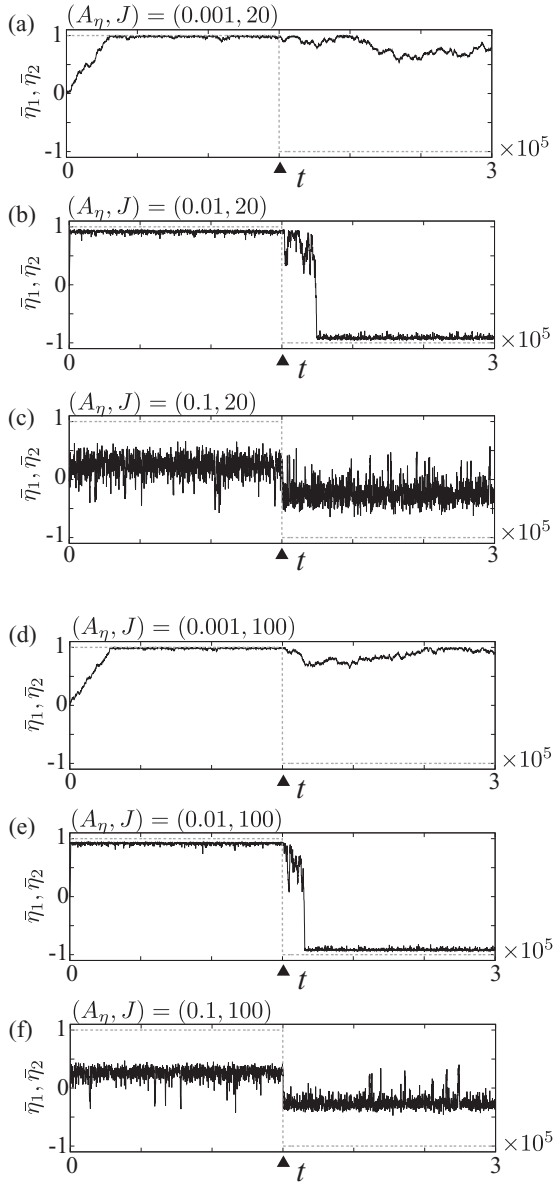
FIG. 6. Examples of time sequences of $\bar{\eta}_1$ (solid black line) and $\bar{\eta}_2$ (dashed gray line) of Eq. (3) when (a) $(A_\eta, J) = (0.001, 20)$, (b) $(A_\eta, J) = (0.01, 20)$, (c) $(A_\eta, J) = (0.1, 20)$, (d) $(A_\eta, J) = (0.001, 100)$, (e) $(A_\eta, J) = (0.01, 100)$, and (f) $(A_\eta, J) = (0.1, 100)$. Triangles indicate the beginning of the perturbations ($t = T/2$).

is replaced by

$$\eta_{lk}^{(j')}(m\tau) = \eta_{lk}^{(j_k^*)}(m\tau), \tag{11}$$

where $j' \in \{1, 2, \ldots, J\}$ is the number of the worst element and $j_k^* = \arg\max_j S_k^{(j)}(m)$. That is, only the parameter values of one element are replaced. Figure 7(b) shows the time sequence of $\bar{\eta}_j$ with Eq. (11), where the experimental settings are the same as those used for Fig. 3(b) except for Eq. (6).

## III. CONTINUOUS MODEL

We propose a continuous model that shows qualitatively the same properties as those of the simple model. In the simple model, the number of oscillators is finite and the selection
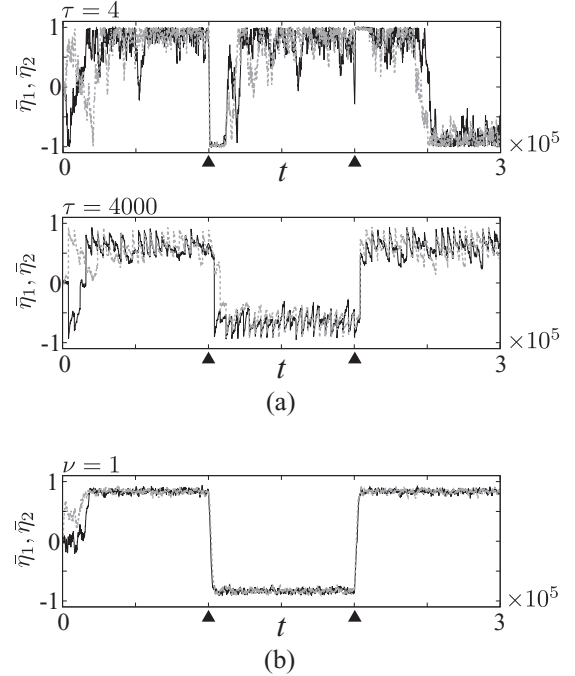


FIG. 7. Examples of time sequences of $\bar{\eta}_1$ (solid black line) and $\bar{\eta}_2$ (dashed gray line) of Eq. (3) when (a) $\tau = 4$ and $\tau = 4000$ and (b) Eq. (11) with $\tau = 100$ is employed. Triangles indicate the beginning of the perturbations: $t = t_1$ and $t_2$.

occurs at every time interval $\tau$. To derive a continuous model, we take the limit $J \to \infty$ and assume that selection occurs at random times. Herein we show a continuous model corresponding to the two-population model shown in Sec. II C.

### A. Continuous model

Because we take the limit $J \to \infty$, we describe the number of oscillators as the density in the parameter space. We define by $\rho_k(t, \eta, \omega)$ the density of oscillators in $P_k$ at time $t$ with the intrinsic parameter values $\eta$ and $\omega$. In our setting, all oscillators in the same population receive the same signal by the mean-field interactions [see Eq. (8)]. Thus it is reasonable to assume that the phases of the oscillators having the same parameter values are equivalent for all $t$, that is, $\boldsymbol{u}_k$ is independent of $\rho_k$. Therefore, we describe the dynamics of the oscillators in population $k$ by

$$\dot{\boldsymbol{u}}_k = \boldsymbol{F}(\boldsymbol{u}_k, \omega_k) + C\eta_k \boldsymbol{U}_{k'} + \boldsymbol{U}_k^{\mathrm{ptb}} + A\boldsymbol{W}_k,$$

$$\boldsymbol{U}_{k'} = \frac{1}{\rho^*} \int_{\eta_{\min}}^{\eta_{\max}} \int_{\omega_{\min}}^{\omega_{\max}} \rho_{k'}(t, \eta, \omega)\boldsymbol{u}_{k'}(t, \eta, \omega)d\eta\, d\omega,$$

where $\boldsymbol{u}_k = {}^t(u_k, v_k)$, $u_k = u_k(t, \eta, \omega)$, $v_k = v_k(t, \eta, \omega)$, $\rho_k = \rho_k(t, \eta, \omega)$, $\rho^* := \iint \rho(\cdot, \eta, \omega)d\eta\, d\omega$, and $(k, k') = (1, 2)$ or $(2, 1)$.

As in the simple model, we use the oscillator amplitude as an order parameter; that is, we take

$$s_k(t, \eta, \omega) = |\boldsymbol{u}_k(t, \eta, \omega)|.$$

The selection process is described by a replicator model [21] in which we use the average of $s_k$:

$$\bar{s}_k(t) = \frac{1}{\rho^*} \int_{\eta_{\min}}^{\eta_{\max}} \int_{\omega_{\min}}^{\omega_{\max}} s_k(t, \eta, \omega) \rho_k(t, \eta, \omega) d\eta \, d\omega.$$

We assume that the density of oscillators with parameters $\eta = \hat{\eta}$ and $\omega = \hat{\omega}$ increases (decreases) if $s_k(\cdot, \hat{\eta}, \hat{\omega}) > \bar{s}_k$ [$s_k(\cdot, \hat{\eta}, \hat{\omega}) < \bar{s}_k$] holds. The parameter fluctuation [noise effect in Eq. (3)] is described by a diffusion equation. Based on these assumptions, we propose a model that we refer to as a reaction-diffusion-replicator system [22,23]

$$\frac{\partial \rho_k}{\partial t} = D_\eta \frac{\partial^2 \rho_k}{\partial \eta^2} + D_\omega \frac{\partial^2 \rho_k}{\partial \omega^2} + \gamma [s_k - \bar{s}_k] \rho_k,$$

$$t > 0, \ \eta \in (\eta_{\min}, \eta_{\max}), \ \omega \in (\omega_{\min}, \omega_{\max}), \quad (12)$$

where $D_\eta$ and $D_\omega$ are the diffusion coefficients and $\gamma$ determines the convergence rate of $s_k$ to $\bar{s}_k$, which corresponds qualitatively to $\tau$ in Eq. (6); large $\gamma$ corresponds to small $\tau$. The parameters are set to $T = 4.0 \times 10^4$, $\mu = -1.0 \times 10^{-4}$, $A = 1.0 \times 10^{-6}$, $D_\eta = 1.6 \times 10^{-5}$, $D_\omega = 4 \times 10^{-8}$, $C = 0.001$, $\gamma = 100$, $(\eta_{\min}, \eta_{\max}) = (-1, +1)$, and $(\omega_{\min}, \omega_{\min}) = (0.1, 0.2)$. The initial data $u(0, \cdot)$ and $v(0, \cdot)$ are taken randomly between $-1$ to $1$, and $\rho(0, \cdot, \cdot) = 1$. We impose the Neumann boundary condition

$$\frac{\partial \rho_k}{\partial \eta}\bigg|_{\eta = \eta_{\min}, \eta_{\max}} = \frac{\partial \rho_k}{\partial \omega}\bigg|_{\omega = \omega_{\min}, \omega_{\max}} = 0.$$

Noted that from Eq. (12) and the Neumann boundary condition, $\rho^*$ is constant, that is,

$$\frac{d}{dt} \int_{\eta_{\min}}^{\eta_{\max}} \int_{\omega_{\min}}^{\omega_{\max}} \rho_k(t, \eta, \omega) d\eta \, d\omega = 0.$$

### B. Results

Similar to Sec. II C, we examine the following two cases. In case 1, the dynamics of $\rho_1$ and $\omega_1$ are described by Eq. (12) while $(\eta_2, \omega_2)$ is fixed at $(\eta_2^*, \omega_2^*)$ and described by using the Dirac $\delta$ function such that $\rho_2$ satisfies

$$\frac{1}{\rho^*} \int_{\eta_{\min}}^{\eta_{\max}} \int_{\omega_{\min}}^{\omega_{\max}} \rho_2(\cdot, \eta_2^*, \omega_2^*) \boldsymbol{u}_2(\cdot, \eta_2^*, \omega_2^*) d\eta \, d\omega = \boldsymbol{u}_2(\cdot, \eta_2^*, \omega_2^*).$$

$$(13)$$

In case 2, the dynamics of $\rho_1$ and $\rho_2$ are described by Eq. (12). For convenience, we define the averages of $\eta_k$ and $\omega_k$ as

$$\bar{\eta}_k = \frac{1}{\rho^*} \int_{\eta_{\min}}^{\eta_{\max}} \int_{\omega_{\min}}^{\omega_{\max}} \rho_k(\cdot, \eta, \omega) \eta \, d\eta \, d\omega,$$

$$\bar{\omega}_k = \frac{1}{\rho^*} \int_{\eta_{\min}}^{\eta_{\max}} \int_{\omega_{\min}}^{\omega_{\max}} \rho_k(\cdot, \eta, \omega) \omega \, d\eta \, d\omega.$$

#### 1. Case 1

For the time integration of the $\rho_1$ equation [Eq. (12)], the spatial grid was taken as $50 \times 50$. Due to Eq. (13), $\boldsymbol{U}_2(t) = {}^t(u_2(t, \eta_2^*, \omega_2^*), v_2(t, \eta_2^*, \omega_2^*))$ holds for all $t$. In addition, $\bar{\eta}_2 \equiv \eta_2^*$ and $\bar{\omega}_2 \equiv \omega_2^*$ hold for all $t$. To confirm the adaptability, we
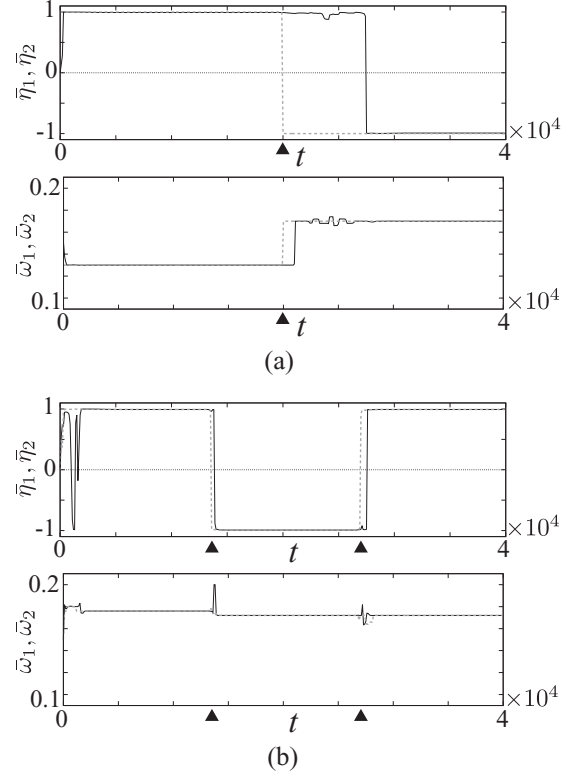


(a)

(b)

FIG. 8. Solid black lines indicate the time sequences of $\bar{\eta}_1$ and $\bar{\omega}_1$ and dashed gray lines indicate the time sequences of $\bar{\eta}_2$ and $\bar{\omega}_2$ for the continuous model. Triangles indicate the beginning of the perturbations: (a) $t = T/2$ and (b) $t = t_1$ and $t_2$.

change $\eta_2^*$ and $\omega_2^*$ as follows:

$$\eta_2^* = \begin{cases} +1 & \text{if } t \leqslant T/2, \\ -1 & \text{if } t > T/2, \end{cases} \quad \omega_2^* = \begin{cases} 0.13 & \text{if } t \leqslant T/2, \\ 0.17 & \text{if } t > T/2. \end{cases}$$

Figure 8(a) shows the typical behavior of the time sequences of $\bar{\eta}_1$ and $\bar{\omega}_1$. We observe that $\bar{\eta}_1$ approaches $+1$ for $t < T/2$ after the transient state at the initial stage, whereupon it approaches $-1$ after the change of $\eta_2^*$ at $t = T/2$. The average of the angular frequency of $P_1$, namely, $\bar{\omega}_1$, follows the time sequence of $\omega_2^*$ even after the parameter is changed.

#### 2. Case 2

Next we consider the case in which both $\rho_1$ and $\rho_2$ are described by Eq. (12). For the time integration of Eq. (12), the spatial grid for the parameter space of $P_1$ and $P_2$ was taken as $50 \times 50$. To confirm the adaptability, we apply the perturbation

$$\boldsymbol{U}_k^{\text{ptb}} = \begin{cases} {}^t(0.1 \ \sin(\omega' t - \theta_k), 0) & \text{if } t \in [t_1, t_1 + t_\delta] \\ {}^t(0.1 \ \sin(\omega' t - \theta_k'), 0) & \text{if } t \in [t_2, t_2 + t_\delta] \\ {}^t(0, 0) & \text{otherwise,} \end{cases} \quad (14)$$

where we set $t_1 = T/3$, $t_2 = 2T/3$, $\omega' = 2$, $t_\delta = 200$, $(\theta_1, \theta_2) = (0, \pi)$, and $(\theta_1', \theta_2') = (0, 0)$.

Figure 8(b) shows that $\bar{\eta}_1$ approaches $+1$ and the populations exhibit in-phase synchronization for $t \in [0, t_1]$. Whether EE or II interactions are selected in $t \in [0, t_1]$ depends on the noise and the initial data. After the external perturbation
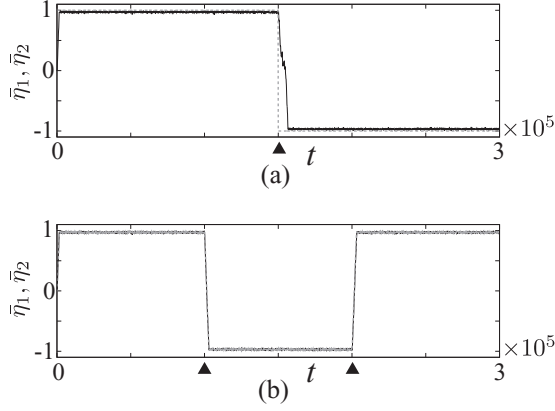
FIG. 9. Solid black and dashed gray lines indicate the time sequences of $\bar{\eta}_1$ (black lines) and $\bar{\eta}_2$ (gray lines). Triangles indicate the beginning of the perturbations: (a) $t = T/2$ and (b) $t = t_1$ and $t_2$. The parameters are set to $T = 3.0 \times 10^5$, $J = 20$, $C = 0.5$, $\omega = 1.0$, $\tau = 100$, and $A_\eta = 0.004$.

at $t = t_1$, the signs of both $\bar{\eta}_1$ and $\bar{\eta}_2$ were changed by the perturbation, which induced antiphase synchronization between $P_1$ and $P_2$. Similarly, the signs of $\bar{\eta}_1$ and $\bar{\eta}_2$ were changed by the perturbation at $t = t_2$, which induced in-phase synchronization between $P_1$ and $P_2$. In addition, it is found that $\bar{\omega}_1$ follows the time sequence of $\bar{\omega}_2$ even after the perturbation was applied.

These results indicate that parameter changes occur quickly following the external perturbation of Eq. (14). For both cases 1 and 2, the results are consistent with those for the simple model shown in Sec. II C.

## IV. DISCUSSION

We proposed a model framework for the emergence of synchronized oscillations. The advantage of our framework is that the formulation of the algorithm is independent of the variables corresponding to the other populations. Because of this property, the same algorithm could be applied to the two-population system and the four-population system. This also means that we do not need to change the algorithm according to the change in the environment. We expect the algorithm to enable robots to adapt to unpredictable environmental changes because the formulation of the algorithm is independent of the variables corresponding to the environment. Owaki *et al.* [17] used an oscillator model and took advantage of the resonance phenomenon that occurs through the robot-environment interaction. We have developed their concept such that the population can control the sign of interactions and the angular frequency, whereas the model in [17] was restricted to controlling the angular frequency. The key point of our framework is that the model generates attractors of the dynamical system involving the parameter-tuning algorithm. In other words, the parameter tuning is accomplished by the convergence of the solution orbit to one of the attractors. For this, the model autonomously finds appropriate parameter values and generates synchronized oscillation. As discussed in Sec. II E, the loop structure of interaction networks between the population and the system was crucial for our framework. Because of the loop

structure, synchronization and desynchronization occur when both populations choose appropriate and inappropriate values, respectively.

In [16,17], the degree of resonance was used to evaluate the performance of systems. In our model, the degree of resonance can be used as an order parameter. A possible formulation is given by

$$S_k^{(j)} = u_k^{(j)} U_{k'},\qquad(15)$$

where $(k, k') = (1, 2)$ or $(2,1)$. We examined the same numerical experiments as those in Sec. II B. Figure 9 shows examples of the time sequence of Eq. (3) when Eq. (15) is used instead of Eq. (4). It is found that the system with Eq. (15) exhibits adaptability against parameter changes. However, we did not use Eq. (15) because the order parameter of the oscillator in $P_k$ depends on the dynamics of the other systems ($U_{k'}$), which is beyond our problem setting.

A large number of mathematical models of locomotor systems describe the phase of the leg motion by coupled oscillator systems. In such models, so that the locomotor system can adapt to external perturbations, the oscillatory pattern should be changed according to the leg motion. That is, the leg motion should regulate the central pattern generator dynamics. The difficulty is how to describe the oscillatory dynamics by using the variables corresponding to the leg motion. As shown in Fig. 4, we succeeded in showing that the oscillator dynamics can control the interaction parameter
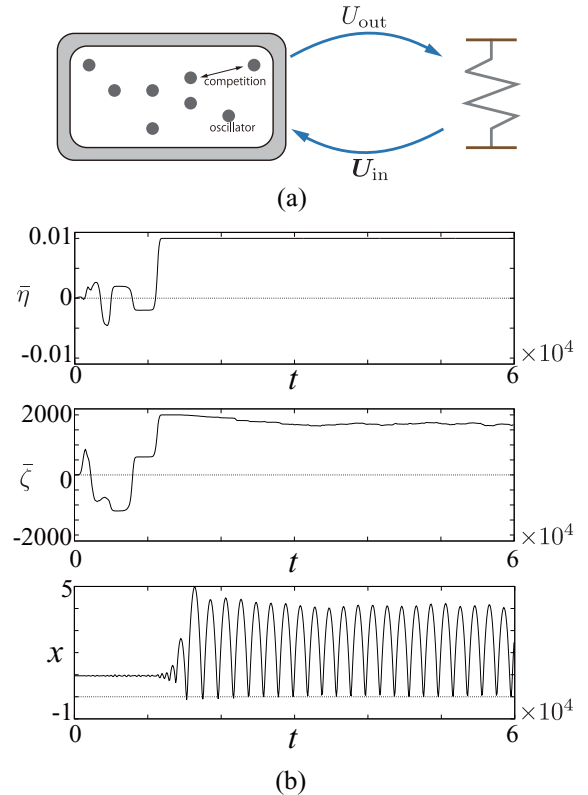


FIG. 10. (a) Model framework. (b) Time sequences of $\bar{\eta}$, $\bar{\zeta}$, and $x$. The parameters are set to $C = 10^{-6}$, $A = 1.0 \times 10^{-5}$, $\eta_{\max} = -\eta_{\min} = 0.01$, $\zeta_{\max} = -\zeta_{\min} = 2000$, $\ell = 1$, $\gamma = 10$, $D_\eta = 1 \times 10^{-9}$, $D_\zeta = 4$, $k_1 = 0.1$, $k_2 = 200$, $\nu = 1000$, and $g = 9.8$.

$\eta_{lk}^{(j)}$. We expect that our algorithm can be applied to the autonomous control of locomotor systems.

In [17] it was shown that the online parameter-tuning system automatically amplifies the oscillation of the spring-damper system. We consider a similar model setting. Here we use the sign and strength of the input $\boldsymbol{U}_{\text{in}}$ and output $U_{\text{out}}$ of the population as control parameters [Fig. 10(a)]. The governing equation is described by

$$\dot{\boldsymbol{u}} = \boldsymbol{F}(\boldsymbol{u}, \omega) + C\eta\boldsymbol{U}_{\text{in}} + A\boldsymbol{W}, \tag{16}$$

$$\boldsymbol{U}_{\text{in}} = {}^{t}(x - \bar{x}, 0),$$

$$U_{\text{out}} = \int_{\eta_{\min}}^{\eta_{\max}} \int_{\zeta_{\min}}^{\zeta_{\max}} \zeta \rho(t, \eta, \zeta) u(t, \eta, \zeta) d\eta \, d\zeta,$$

$$s = |\boldsymbol{u}|,$$

$$\bar{s} = \frac{1}{\rho^*} \int_{\eta_{\min}}^{\eta_{\max}} \int_{\zeta_{\min}}^{\zeta_{\max}} s(t, \eta, \zeta)\rho(t, \eta, \zeta) \, d\eta \, d\zeta,$$

$$\frac{\partial \rho}{\partial t} = D_\eta \frac{\partial^2 \rho}{\partial \eta^2} + D_\zeta \frac{\partial^2 \rho_k}{\partial \zeta^2} + \gamma[s - \bar{s}]\rho,$$

$$x'' = \begin{cases} -k_1 x' - k_2(x - \ell) - g + U_{\text{out}} & \text{if } x \leqslant \ell \\ -g & \text{otherwise,} \end{cases}$$

$$t > 0, \ \eta \in (\eta_{\min}, \eta_{\max}), \ \zeta \in (\zeta_{\min}, \zeta_{\max}), \tag{17}$$

where the prime indicates the derivative with respect to $\tilde{t} = \nu t$, $\ell$ is the natural length of the spring, $k_1$ is the friction coefficient, $k_2$ is the spring coefficient, $g$ is the gravitational acceleration, $\boldsymbol{u}_k = {}^{t}(u_k, v_k), u_k = u_k(t, \eta, \zeta), v_k = v_k(t, \eta, \zeta),$

$\rho_k = \rho_k(t, \eta, \zeta), \rho^* := \iint \rho(\cdot, \eta, \zeta)d\eta \, d\zeta$, and $\bar{x} = \ell - g/k_2$. The parameter $\nu > 0$ is introduced to adjust the time scale of the oscillators (16) and the spring-damper system (17). We impose the Neumann boundary condition

$$\frac{\partial \rho}{\partial \eta}\bigg|_{\eta=\eta_{\min},\eta_{\max}} = \frac{\partial \rho}{\partial \zeta}\bigg|_{\zeta=\zeta_{\min},\zeta_{\max}} = 0.$$

Figure 10(b) shows time sequences of $\bar{\eta}$ and $\bar{\zeta}$, where

$$\bar{\eta} = \frac{1}{\rho^*} \int_{\eta_{\min}}^{\eta_{\max}} \int_{\zeta_{\min}}^{\zeta_{\max}} \rho(\cdot, \eta, \zeta)\eta \, d\eta \, d\zeta,$$

$$\bar{\zeta} = \frac{1}{\rho^*} \int_{\eta_{\min}}^{\eta_{\max}} \int_{\zeta_{\min}}^{\zeta_{\max}} \rho(\cdot, \eta, \zeta)\zeta \, d\eta \, d\zeta.$$

It is found that the amplitude of the spring-damper system is increased by appropriate parameter controls.

In this paper, we proposed a general framework for the self-organization of a synchronized oscillator system involving appropriate parameter choices. It was found that a simple algorithm enables the system to find appropriate parameter values to generate synchronized oscillations. We expect that this study will motivate a new experimental setting to elucidate the self-organization process in biological systems.

[1] J. J. Hopfield, Proc. Natl. Acad. Sci. USA **81**, 3088 (1984).

[2] Q. Ren and J. Zhao, Phys. Rev. E **76**, 016207 (2007).

[3] M. Chen, Y. Shang, Y. Zou, and J. Kurths, Phys. Rev. E **77**, 027101 (2008).

[4] T. Aoki and T. Aoyagi, Phys. Rev. Lett. **102**, 034101 (2009).

[5] T. Aoki and T. Aoyagi, Phys. Rev. E **84**, 066109 (2011).

[6] S. Assenza, R. Gutiérrez, J. Gómez-Gardenes, V. Latora, and S. Boccaletti, Sci. Rep. **1**, 99 (2011).

[7] W. Yu, P. DeLellis, G. Chen, M. Di Bernardo, and J. Kurths, IEEE Trans. Autom. Control **57**, 2153 (2012).

[8] T. Gross and B. Blasius, J. R. Soc. Interface **5**, 259 (2007).

[9] T. Aoki and T. Aoyagi, Phys. Rev. Lett. **109**, 208702 (2012).

[10] H. Nijmeijer and I. M. Y. Mareels, IEEE Trans. Circuits Syst. I **44**, 882 (1997).

[11] T. L. Liao and S. H. Tsai, Chaos Solition. Fractal. **11**, 1387 (2000).

[12] J. H. Park, Chaos Solition. Fractal. **26**, 959 (2005).

[13] S. Sinha and N. Gupte, Phys. Rev. E **58**, R5221 (1998).

[14] I. Z. Kiss, C. G. Rusin, H. Kori, and J. L. Hudson, Science **316**, 1886 (2007).

[15] G. Taga, Y. Yamaguchi, and H. Shimizu, Biol. Cybern. **65**, 147 (1991).

[16] J. Buchli and A. J. Ijspeert, Autonomous Robots **25**, 331 (2008).

[17] D. Owaki, S. Ishida, A. Tero, K. Ito, K. Nagasawa, and A. Ishiguro, Adv. Robot. **25**, 1139 (2011).

[18] A. T. Winfree, *The Geometry of Biological Time*, Interdisciplinary Applied Mathematics Vol. 12 (Springer Science + Business Media, New York, 2001).

[19] G. Gerisch and B. Hess, Proc. Natl. Acad. Sci. USA **71**, 2118 (1974).

[20] J. J. Collins and S. A. Richmond, Biol. Cybern. **71**, 375 (1994).

[21] J. Hofbauer and K. Sigmund, *The Theory of Evolution and Dynamical Systems: Mathematical Aspects of Selection* (Cambridge University Press, New York, 1988).

[22] A. S. Bratus, V. P. Posvyanskii, and A. S. Novozhilov, Math. Model. Nat. Pheno. **9**, 47 (2014).

[23] A. S. Novozhilov, V. P. Posvyanskii, and A. S. Bratus, Russ. J. Numer. Anal. Math. Model. **26**, 555 (2012).